Journal of
Composites Science

MDPI

Article

Calcium-Structured Alginate Hydrogels: Network Formation, Rheology, Swelling, and Collagen Release

Nataliia Nosova [1,*], Olha Maikovych [1], Olena Bordeniuk [1], Solomiia Kapatsila [1], Roman Taras [1], Nataliia Bukartyk [1], Yuliia Cherkas [1], Anna Stasiuk [1], Semen Khomyak [1], Dmytro Ostapiv [2], Volodymyr Samaryk [1] and Serhii Varvarenko [1]

[1] Department of Organic Chemistry, Lviv Polytechnic National University, 12 Bandera Str., 79013 Lviv, Ukraine; olha.v.maikovych@lpnu.ua (O.M.); olena.y.bordeniuk@lpnu.ua (O.B.); solomiia.m.kapatsila@lpnu.ua (S.K.); roman.s.taras@lpnu.ua (R.T.); nataliia.m.bukartyk@lpnu.ua (N.B.); yuliia.cherkas.mkhtkhd.2026@lpnu.ua (Y.C.); anna.v.stasiuk@lpnu.ua (A.S.); semen.v.khomyak@lpnu.ua (S.K.); volodymyr.y.samaryk@lpnu.ua (V.S.); serhii.m.varvarenko@lpnu.ua (S.V.)
[2] Institute of Animal Biology NAAS, 38 V. Stusa Str, 79034 Lviv, Ukraine; oddost@ukr.net
* Correspondence: nataliia.h.nosova@lpnu.ua

Abstract

Combined hydrogels based on interpenetrating polymer networks of sodium alginate, hydrolyzed collagen, hydroxypropyl methylcellulose, and the calcium salt of lightly crosslinked poly(acrylic acid) were developed for potential use as wound dressings. The effects of the alginate-to-collagen ratio on network formation and the functional properties of the materials were evaluated by extraction-based gel-fraction determination, Fourier-transform infrared spectroscopy, mechanical and rheological measurements, swelling studies in water and simulated wound exudate, collagen-release analysis, and in vitro cytocompatibility assessment. Extraction analysis and spectroscopic data confirmed the incorporation of collagen into the polymer network and revealed a nonlinear relationship between composition and network-formation efficiency. Structural stability was governed by the balance between calcium-mediated ionic crosslinking, electrostatic interactions, and hydrogen bonding, whereas an excess of unbound low-molecular-weight collagen fragments reduced the insoluble network fraction. All hydrogels exhibited predominantly elastic behavior, while their stiffness and mechanical strength varied nonmonotonically with the biopolymer ratio. Swelling was determined by network composition and density; in simulated wound exudate, ionic screening, limited matrix expansion and promoted shape retention. Collagen-release kinetics were also composition-dependent: a more hydrophilic, mobile, alginate-rich network provided faster release, whereas a higher collagen content promoted prolonged diffusion. Cytocompatibility assessment of the representative formulation (Sample 2) indicated no reduction in cell viability in the applied in vitro model, although alterations in oxidative enzyme activity were observed. These findings demonstrate that the structural, mechanical, sorption, and release properties of alginate–collagen hydrogels can be tailored for the development of promising wound dressings.

Keywords: sodium alginate; hydrolyzed collagen; lightly crosslinked poly(acrylic acid) calcium salt; hydrogel wound dressings; collagen release

Check for updates

Academic Editors: Mani Ganesh and Jayabalan Jayaprakash

Received: 2 October 2026
Revised: 23 October 2026
Accepted: 27 October 2026
Published: 13 November 2026

Copyright: © 2026 by the authors. Licensee MDPI, Basel, Switzerland. This article is an open access article distributed under the terms and conditions of the Creative Commons Attribution (CC BY) license.

1. Introduction

Hydrogel wound dressings are widely investigated for the management of diverse skin injuries [1,2]. The global market for hydrogel dressings exceeded USD 920 million in

2023 and is projected to reach approximately USD 1–1.33 billion by 2030, driven primarily by the increasing prevalence of chronic wounds, population aging, and advances in medical technologies [3]. Products for chronic wounds, including diabetic foot ulcers, venous ulcers, and pressure ulcers, account for approximately 60% of use. The acute-wound segment, encompassing burns, surgical wounds, and traumatic injuries, represents 20% of the market and is projected to grow by approximately 4.5% annually [4]. Hydrogel wound dressings should absorb exudate, permit air and water-vapor transport, maintain an appropriate moisture balance, limit infection, avoid irritation and allergic responses, and provide adequate mechanical performance [5–8]. Despite extensive research, materials with improved and application-specific properties remain in demand [9–13]. The main direction of current research in this field is the development of wound dressings based on natural renewable raw materials. This trend is driven by several factors: biocompatibility, since natural polymers such as chitosan, alginate, and collagen are generally non-toxic and do not induce allergic reactions; biodegradability, because natural hydrogel wound dressings can degrade in the body into safe products, eliminating the need for mechanical removal from the wound and reducing damage to newly formed tissue; bioactivity, since many natural substances possess intrinsic therapeutic properties, accelerate cell regeneration, and exhibit antibacterial activity; and environmental sustainability and availability, as renewable raw materials can make production less costly and less harmful to the environment [14–17].

However, individual polymer hydrogels are generally unable to fully satisfy all clinical requirements due to their severe intrinsic limitations; therefore, the search for optimal solutions in the field of hybrid or combined systems is ongoing. Specifically, pure sodium alginate hydrogels, despite their excellent exudate absorption, exhibit pronounced mechanical brittleness, poor structural stability in physiological fluids due to rapid displacement of crosslinking cations, and a lack of specific cell-adhesion motifs to actively drive tissue regeneration. On the other hand, while hydrolyzed collagen provides exceptional biological activity and may provide biological functions relevant to the extracellular matrix, its low-molecular-weight peptide fragments (5000–10,000 Da) are entirely incapable of forming a stable, standalone three-dimensional hydrogel network, leading to immediate dissolution and premature leaching upon contact with wound fluids.

The incorporation of several natural polymers, or biopolymers, into wound dressings makes it possible to obtain materials with synergistic effects, in which each component compensates for the limitations of the others while contributing its own functional advantages. Such systems may provide the following benefits: (1) improved mechanical performance and reduced brittleness [18]; (2) precise regulation of moisture content and water-retention capacity [19]; (3) achievement of complex biological activity, where alginate creates a barrier and a moist environment while collagen peptides actively stimulate cell migration and metabolic rearrangements [20–22]; (4) controlled biodegradation and bioresorption rates; and [23,24]; and (5) enhanced biocompatibility by closely mimicking the native multi-component extracellular matrix [25].

Although composite hydrogels based on sodium alginate and gelatin cross-linked with various agents, including our previously developed calcium salt of lightly cross-linked poly(acrylic acid) (LC-PAA-Ca) have shown potential, they often suffer from processing limitations due to the high viscosity and macromolecular rigidity of intact gelatin. The scientific advance of this work lies in the strategic replacement of high-molecular-weight biopolymers with low-molecular-weight hydrolyzed collagen (5000–10,000 Da) in an interpenetrating network structured by the synthesized LC-PAA-Ca. Due to the low viscosity of hydrolyzed collagen at elevated concentrations, highly homogeneous precursor mixtures can be achieved. In addition, the high segmental mobility of these peptide fragments alters the thermodynamics of crosslinking, promoting cooperative hydrogen bonding and poly-

electrolyte interactions with the LC-PAA matrix, while modulating the ionotropic gelation of alginate.

Therefore, the aim of this study was to develop composite hydrogels based on alginate and hydrolyzed collagen and determine the effects on network formation, rheological behavior, swelling profiles in water and simulated wound exudate, sustained release of collagen peptides, and in vitro cytocompatibility for potential advanced wound dressing applications.

2. Materials and Methods

2.1. Materials

Hydrolyzed collagen (Aminosens Collagen Powder, yellow powder, commercial grade, NATURA-TEC, Fréjus, France, CAS 92113-31-0; obtained via controlled enzymatic hydrolysis of bovine connective tissues, primarily types I and III collagen, with a molecular weight range of 5000–10,000 Da), sodium alginate (white powder, CAS 9005-38-3), and hydroxypropyl methylcellulose (HPMC, white powder, commercial grade METHOCEL™ 267, Dow Chemical, Midland, MI, USA, CAS 9004-65-3) were used as received without further purification.

Lightly crosslinked poly(acrylic acid) (LC-PAA) and its calcium salt (LC-PAA-Ca), used as structuring agents, were prepared according to the procedure described previously [26]. The Ca^{2+} content in LC-PAA-Ca was 15%.

Polyethylene glycol with a nominal molar mass of 400 Da (PEG-400, Aldrich, St. Louis, MO, USA, CAS 25322-68-3) and glycerol (Aldrich, CAS 56-81-5) were used without additional purification.

Calcium chloride (CAS 10043-52-4), sodium chloride (CAS 7647-14-5), and 2-amino-2-(hydroxymethyl)propane-1,3-diol (TRIS, CAS 77-86-1) were used as received.

Bovine serum albumin (BSA, lyophilized powder, ≥96% by agarose gel electrophoresis, Aldrich A2153, CAS 9048-46-8) was used without further purification.

Distilled water with a density of $\rho = 0.998$ g cm^{-3} at 20 °C, a refractive index of $n = 1.333$ at 20 °C, and a specific electrical conductivity below 10 μS cm^{-1} was used throughout the experiments.

A standard pH 7.00 buffer solution based on disodium hydrogen phosphate/potassium dihydrogen phosphate (Merck, Rahway, NJ, USA) was used for pH control.

The model wound exudate was prepared according to the procedure reported previously [27]: 8.035 g of NaCl, 0.292 g of $CaCl_2$, and 6.118 g of 2-amino-2-(hydroxymethyl)propane-1,3-diol (TRIS) were dissolved in 100 mL of distilled water. Subsequently, 20 g of a 5% aqueous bovine serum albumin (BSA) solution was added, and the volume was adjusted to the 1L with distilled water. The resulting solution was stored in the refrigerator at 2–4 °C and was suitable for use within 7 days.

The bovine spermatozoa used in this study were obtained from the Lviv Scientific and Production Center "Zakhidplemresursy" LLC (Lviv, Ukraine).

2.2. Preparation of Alginate–Collagen Hydrogels

Alginate–collagen hydrogels were prepared using two precursor systems: (i) aqueous solutions of hydrolyzed collagen and sodium alginate in distilled water at different component ratios (Table 1), and (ii) a dispersion containing the calcium salt of lightly crosslinked poly(acrylic acid) (LC-PAA-Ca, 5%), poly(acrylic acid) (LC-PAA, 0.5%), HPMC (5%), glycerol (44.75%), and PEG-400 (44.75%).

Table 1. Initial concentrations of sodium alginate and hydrolyzed collagen in the precursor solutions.

Sample ID	Initial Sodium Alginate Concentration (wt.%)	Initial Hydrolyzed Collagen Concentration (wt.%)
Sample 1	3.05	0.00
Sample 2	3.05	1.26
Sample 3	3.05	6.39
Sample 4	3.04	12.76
Sample 5	0.00	3.04
Sample 6	2.16	2.16
Sample 7	1.26	3.05
Sample 8	2.76	1.58
Sample 9	1.55	2.76

To synthesize the hydrogels, the corresponding alginate–collagen solution and the structuring dispersion were thoroughly blended in a strict 4:1 mass ratio (specifically, 80 g of the biopolymer solution was combined with 20 g of the dispersion to yield a total precursor mass of 100 g). The mixture was stirred continuously for 3 min to ensure absolute homogeneity, cast into square Petri dishes 10 ×10 cm, hermetically sealed, and allowed to undergo ionotropic gelation at 20 °C for 5 h. Subsequently, the hydrogels were transferred to a drying oven and dehydrated at 40 °C under gravimetric control until a target residual moisture content was achieved (Table 2), resulting in uniform hydrogel plates with a final thickness of 3.0 ± 0.1 mm.

Table 2. Percentage composition of alginate–collagen hydrogels.

Hydrogel Composition	Sample Number								
	1	2	3	4	5 *	6	7	8	9
Sodium alginate	3.74	3.71	3.60	3.48	0.00	2.63	1.54	3.37	1.90
HPMC	1.55	1.54	1.50	1.45	1.55	1.53	1.53	1.53	1.53
LC-PAA-Ca	1.56	1.55	1.50	1.45	1.55	1.53	1.53	1.53	1.53
Water	65.16	63.87	58.81	52.89	65.26	64.13	64.13	64.11	64.13
Glycerol	13.90	13.80	13.42	12.97	13.86	13.68	13.68	13.68	13.68
PEG-400	13.93	13.84	13.45	13.00	13.89	13.71	13.71	13.71	13.71
LC-PAA	0.16	0.15	0.15	0.15	0.16	0.15	0.15	0.15	0.15
Hydrolyzed collagen	0.00	1.54	7.57	14.62	3.73	2.63	3.72	1.92	3.37
Total	100.0	100.0	100.0	100.0	100.0	100.0	100.0	100.0	100.0
Total concentration of gel-forming polymers	5.46	6.96	12.82	19.70	5.44	6.95	6.95	6.98	6.95
Mass ratio of sodium alginate to hydrolyzed collagen	-	2.41	0.48	0.24	0.00	1.00	0.41	1.75	0.56

* No hydrogel was formed.

Hydrogel formation is primarily attributed to Ca^{2+}-mediated ionic crosslinking of sodium alginate:

$$2\mathrm{Alg}-\mathrm{COO}^{-}\mathrm{Na}^{+}+\mathrm{Ca}^{2+}\rightleftharpoons(\mathrm{Alg}-\mathrm{COO}^{-})_{2}\mathrm{Ca}^{2+}+2\mathrm{Na}^{+}$$

The calcium ions supplied by LC-PAA-Ca can coordinate with carboxylate groups of alginate chains, promoting the formation of ionic junction zones commonly described by the egg-box model. Hydrolyzed collagen is expected to be incorporated into the polymer

network predominantly through physical interactions, including possible hydrogen bonding and electrostatic interactions with the other polymer components. No specific covalent crosslinking reaction involving collagen was employed during hydrogel preparation.

Moisture Content Control and Determination

To verify and control the target residual water content during the dehydration process, a gravimetric method was employed. Three representative square specimens (2 × 2 cm) were cut from different zones of the drying hydrogel plate and weighed immediately to determine their initial mass (m_0, g). The specimens were then heated in a drying oven at 100 °C for 2 h to eliminate all volatile moisture, cooled to room temperature in a desiccator over a silica gel desiccant, and reweighed to obtain the constant dry mass (m_t, g). The residual moisture content (W, %) was calculated according to the following Equation (1):

$$W(\%) = \frac{m_0 - m_t}{m_0} \times 100\% \quad (1)$$

where m_0 is the mass of the hydrogel specimen before dehydration analysis (g), and m_t is the dry mass of the specimen after drying at 100 °C to constant weight (g).

The final moisture content of each hydrogel patch was reported as the mean value of three parallel replicates.

2.3. Swelling Study of the Hydrogels

The degree of swelling of the alginate–collagen hydrogels were determined gravimetrically in distilled water and simulated wound exudate at 20 ± 1 °C and 36 ± 0.5 °C.

Cylindrical hydrogel specimens (0.9 cm in diameter and 0.35 cm in height), each weighing approximately 0.22–0.25 g, were used. Each specimen was placed in a weighing bottle and weighed on an analytical balance with a readability of 0.0001 g to determine its initial mass, m_0. The specimens were then immersed in the respective swelling medium. At predetermined time points (3, 24, 50/52, 98, and 140/148 h), the specimens were removed from the medium, gently blotted with a lint-free tissue to remove excess surface liquid, and weighed to determine the swollen mass at time t, m_t.

Since the initial hydrogel matrix contained a substantial amount of water and highly water-soluble plasticizers (glycerol and PEG-400), immersion into an excess of an external liquid induces a simultaneous dual-diffusion process: the osmotic influx of fluid into the network and the competitive leaching (efflux) of these soluble components into the surrounding medium. Consequently, the gravimetric values capture a combined mass-transfer profile rather than idealized polymer network expansion. To accurately reflect this macroscopic performance, the parameter is defined as the apparent (net) swelling degree, (α, %), and was calculated using the following Equation (2):

$$\alpha(\%) = \frac{m_t - m_0}{m_0} \times 100 \quad (2)$$

where m_t is the mass of the swollen specimen at time t (g), and m_0 is the initial hydrogel mass (g).

Therefore, the calculated apparent degree of swelling represents the relative net sorption capacity of the completely formulated, commercial-ready hydrogel patch during direct contact with excess external liquid within the investigated boundary conditions. All measurements were performed in triplicate ($n = 3$), and the results are reported as mean values with standard deviations ($M \pm$ SD).

2.4. Determination of Gel Fraction Content

The gel fraction, G_f (%), of the hydrogel specimens was determined by water extraction using the tea-bag method. The tea bags were dried in an oven to constantly mass, m_p. A

hydrogel specimen with an initial mass, m_0, of approximately 3.0 g was weighed with a readability of 0.0005 g, placed in a tea bag, and sealed.

The sol fraction was extracted in a large excess of distilled water at a specimen-to-water mass ratio of 1:500 for 24 h at 45 ± 1 °C. To maintain a high concentration gradient and ensure exhaustive extraction, the water was completely replaced with a fresh portion every 3 h.

After extraction, the tea bags were removed and dried in an oven at 50 ± 1 °C to constant mass, m_d.

The gel fraction, G_f (%), was calculated as the ratio of the dry residue mass to the initial total mass of gel-forming polymers in the hydrogel using the following Equation (3):

$$G_f(\%) = \frac{m_d - m_p}{m_0 \times w/100} \times 100 \quad (3)$$

where m_d is the constant mass of the bag containing the dried gel fraction (g);

m_p is the mass of the empty dry bag (g);

m_0 is the initial hydrogel sample mass (g);

w is the total mass fraction of gel-forming polymers in the corresponding hydrogel composition (%).

Measurements were performed using four independent specimens ($n = 4$), and the results were average.

2.5. Determination of the Mechanical Properties of Hydrogel Samples

2.5.1. Uniaxial Compression Testing

The mechanical resistance of the hydrogel samples was evaluated by stepwise uniaxial compression using a custom-built testing apparatus, following the procedure described in [26]. Cylindrical hydrogel specimens with a diameter of 12 mm and a height of 3 mm were tested without additional pretreatment. Each specimen was placed on a temperature-controlled light-weight metal block mounted on an electronic balance. The block was connected to an external circulating water thermostat set to 36 °C, providing heating to the specimen from below.

Compression was applied manually using a vertically movable plunger in successive displacement increments of 0.5 mm, controlled by a graduated displacement scale. After each increment, the plunger position was held constant for 5 min, during which the balance readings with a readability of 1 g were recorded at 1 min intervals. The onset of specimen failure was identified primarily by an abrupt change in the recorded load, supported by visual observation of structural damage.

The maximum compressive stress (σ_{max}) was calculated from the maximum recorded load prior to specimen failure, normalized by the initial cross-sectional area of the hydrogel specimen, according to Equation (4):

$$\sigma_{\max} = \frac{4m_{\max}g}{\pi(0.012)^2 \cdot 1000} \quad (4)$$

where σ_{max} is the maximum compressive stress (kPa), m_{max} is the maximum mass-equivalent reading recorded by the electronic balance before specimen failure (kg), g is the gravitational acceleration (9.81 m/s^2), and 0.012 is the initial specimen diameter (m). The factor of 1000 converts the calculated stress from Pa to kPa.

2.5.2. Oscillatory Rheological Measurements

The viscoelastic properties of the hydrogel samples were investigated using a modified procedure based on [27]. Rheological measurements were performed using a HAAKE

MARS iQ rheometer (Thermo Scientific, Waltham, MA, USA) equipped with a 25 mm parallel-plate geometry. Disk-shaped hydrogel specimens (25 mm in diameter and approximately 3 mm in height) were placed between the plates. The measurement gap was adjusted to the specimen height until a normal force of 0.15 N was reached, ensuring contact between the upper plate and the sample surface.

Prior to frequency-sweep measurements, strain-amplitude sweeps were performed for each hydrogel formulation in controlled-deformation mode over a strain-amplitude range (γ_0) of 0.001–15 (dimensionless) at a constant frequency of 1 Hz and a temperature of 20 °C. The linear viscoelastic region (LVER) was identified from the plateau of the storage modulus (G'), where G' remained approximately independent of strain amplitude. The corresponding stress-amplitude dependence was then examined to select an appropriate stress amplitude for subsequent measurements. A stress amplitude (τ_0) of 500 Pa was confirmed to lie within the LVER of all investigated formulations at 1 Hz.

Frequency-sweep measurements were subsequently performed in controlled-stress mode at a constant stress amplitude of 500 Pa over a frequency range of 0.1–20 Hz at 20 °C. The storage modulus (G') and loss modulus (G'') were recorded as frequency functions. Experimental data were processed using HAAKE RheoWin 4 software (version: 4.94.0000, Tewksbury, MA, USA). Data exhibiting evidence of cohesive gel failure or interfacial slippage were excluded from the analysis.

2.6. Cytotoxicity Assessment of Hydrogel Samples

The cytotoxicity of the hydrogel samples was assessed according to the procedure described in [26]. The cytotoxicity of the hydrogels was assessed by incubating bovine spermatozoa in direct contact with the samples. Ejaculates selected for the study met the following physiological criteria: volume of 3–4 mL, sperm concentration of 6–11 × 10^8 cells/mL, and a viability rate (live germ cells) of 80–85%.

Sperm samples were divided into two groups: the control with dissolved phosphate-salt buffer, including NaCl—0.8 g, KCl—0.02 g, Na_2HPO_4—0.11 g, KH_2PO_4—0.02 g, $MgCl_2$—0.01 g, distilled water–up to 100 mL, and experimental. Hydrogels were added to the experimental samples at 10, 20, and 50 mg/mL diluted sperm.

Indicators characterising the course of redox processes in germ cells were determined, in particular: succinate dehydrogenase activity (SDH, units) using 2,3,5-triphenyl tetrazolium chloride and cytochrome oxidase (CHO, units) with "Nadi" reagent. The cytotoxicity of the obtained combined hydrogels was evaluated by the duration of sperm survival (h) using a microscope (×200) until linear translational motion in semen stored at a temperature of 2–5 °C is observed. Cytotoxicity analysis based on the retention of sperm motility was performed at varying intervals: every 24 h when up to 50% of cells exhibited progressive motility, every 12 h when this figure was up to 10%, and hourly when the value fell below 10%.

2.7. Fourier-Transform Infrared Spectroscopy

Fourier-transform infrared (FTIR) spectra were recorded using a Spectrum Two spectrometer (PerkinElmer, Liantrisant, UK) equipped with a universal attenuated total reflectance accessory and a diamond crystal. Spectra were acquired over the range 4000–400 cm^{-1} at a resolution of 4 cm^{-1}, with 16 scans collected per spectrum. Spectra were processed using PerkinElmer Spectrum 10 software (version: 10.7.2, Shelton, CT, USA) and assigned using standard correlation tables of characteristic absorption frequencies [28].

2.8. Investigation of Collagen Release from Alginate–Collagen Hydrogels into Different Media

A cylindrical alginate–collagen hydrogel specimen (3.0 mm thick and 2.25 cm in diameter) was weighed and placed into a release medium (distilled water or simulated wound exudate) at a specimen-to-medium mass ratio of 1:10. The release process was conducted at a constant temperature of 36 °C, maintained throughout the experiment using a thermostat. At specified time intervals (1, 2, 4, 6, 7, 8, 14, 18, and 24 h), 1 mL aliquots were withdrawn from the medium. To maintain a constant total volume and ensure sink conditions, each withdrawn volume was immediately replaced with 1 mL of fresh medium (distilled water or simulated exudate, respectively).

Before measurement, aliquot (1 mL) was diluted with an appropriate medium (4 mL, a 5-fold dilution). The optical density of the withdrawn aliquots was measured at a wavelength of $\lambda = 276.1$ nm using a ULAB 108 UV spectrophotometer (Nanjing, China) in a quartz cuvette with an optical path length of 10 mm.

Collagen concentrations were calculated from the calibration equations $C_w = (D - 0.0052)/1.3775$ for distilled water and $C_{ex} = (D + 0.0066)/1.3838$ for simulated wound exudate. Since the selection of aliquots constantly reduces the amount of collagen in the system, the cumulative mass of released collagen (m_t) at time t was calculated according to Equation (5):

$$m_t = C_t V_0 + V_a \sum_{i=1}^{t-1} C_i \quad (5)$$

where C_t is the collagen concentration in the medium at time t, mg/mL;

V_0 is the total volume of the release medium, mL;

V_a is the volume of the aliquot withdrawn ($V_a = 1$ mL);

C_i is the collagen concentration determined at previous time intervals, mg/mL.

The collagen release n was calculated as the ratio of the mass of collagen released from the specimen at time t to the initial collagen mass in the hydrogel using the following Equation (6):

$$n\ (\%) = \frac{m_t}{m_0} \times 100 \quad (6)$$

where m_t is the mass of collagen released from the specimen at time t (g); and m_0 is the initial collagen mass in the hydrogel (g).

To obtain additional insight into the mechanism of collagen release, the experimental release data were fitted to zero-order, first-order, Higuchi, Hixson–Crowell, and Korsmeyer–Peppas kinetic models. The corresponding kinetic parameters were calculated from the linearized forms of the model equations using linear regression analysis. The goodness of fit was evaluated using the coefficient of determination (R^2). For the Korsmeyer–Peppas model, only the initial stage of release corresponding to $Mt/M_\infty < 0.6$ was used, in accordance with the original assumptions of the model. The release exponent n was used to identify the predominant release mechanism.

2.9. Statistical Analysis

All experimental measurements were performed at least in triplicate, and the data are expressed as mean values ± standard deviation ($M \pm$ SD) or mean ± standard error of the mean ($M \pm$ SEM). To evaluate the statistical significance of variations across the multiple hydrogel formulations, a one-way Analysis of Variance (one-way ANOVA) followed by Tukey's post-hoc test was applied for multiple comparisons of gel fraction, swelling kinetics, mechanical properties (maximum compressive stress), rheological parameters (G''/G' ratio), and in vitro collagen release profiles. Student's t-test for independent samples was employed strictly for isolated pair-wise comparisons in biological cytotoxicity assays.

Statistical significance in all tests was defined at ($p < 0.05$). All error bars presented in the figures correspond to the standard deviations calculated from parallel replicates.

3. Results and Discussion

Previous studies from our group investigated sodium alginate-gelatin hydrogels prepared using different crosslinking approaches, including covalent crosslinking with a diepoxide agent [10] and ionotropic structuring based on LC-PAA-Ca [26]. Similar calcium-mediated secondary crosslinking strategies have also been reported for the development of multifunctional hydrogel systems. In particular, the incorporation of calcium ions into poly(acrylic acid) networks chemically crosslinked with N,N′-methylenebisacrylamide (MBA) has been shown to generate additional reversible ionic junctions within PAA-based hydrogels, contributing to their structural adaptability and mechanical performance [29,30]. While LC-PAA-Ca has previously been applied as a structuring agent in alginate–gelatin hydrogels [26], its use in combination with hydrolyzed collagen has not been investigated. In the present study, hydrolyzed collagen was employed as the protein component of the hydrogel matrix instead of gelatin. Owing to its lower molecular weight and higher molecular mobility, hydrolyzed collagen is expected to influence precursor viscosity, intermolecular interactions, and the accessibility of ionizable functional groups involved in network formation. The investigated system therefore combines sodium alginate, hydrolyzed collagen, and LC-PAA-Ca as a dispersed polymeric calcium-releasing phase within a single hydrogel matrix. This combination provides an opportunity to evaluate how controlled calcium release and the specific characteristics of hydrolyzed collagen affect network formation and the resulting physicochemical properties of the hydrogels.

Sodium alginate was selected because of its gel-forming ability, low cost, availability, and extensive investigation as a biomaterial for biomedical applications [28,31,32]. Its carboxylate groups, particularly those of α-L-guluronic acid residues, enable Ca^{2+}-mediated ionotropic gelation according to the classical "egg-box" model [20,33].

Collagen is a major structural protein of the extracellular matrix and is involved in wound-healing processes [34]. Hydrolyzed collagen consists of relatively short peptides whose chemical behavior is governed mainly by glycine, proline, and hydroxyproline residues. Peptide and hydroxyl groups can contribute to hydrogen bonding, whereas carboxyl and amino groups can ionize depending on pH and participate in polyelectrolyte complex formation and ionic crosslinking. These functional groups also increase hydrophilicity and water retention. Unlike gelatin, hydrolyzed collagen remains readily soluble at room temperature and forms comparatively low-viscosity solutions even at high concentrations. This facilitates the preparation of homogeneous precursor mixtures and may influence the distribution of calcium ions and the development of the polymer network during gelation.

Three-dimensional networks based on sodium alginate and hydrolyzed collagen can be formed through interactions with polyvalent metal ions. Conventional salts such as calcium chloride, calcium gluconate, zinc chloride, and aluminum sulfate often induce gelation too rapidly, which can produce structurally heterogeneous materials and hinder control of product shape and dimensions [16,35,36]. Here, LC-PAA-Ca (Figure 1) was used as the structuring agent. As shown previously [26], its use as a 20% dispersion in a PEG/glycerol mixture slows Ca^{2+} release, delays the onset of network formation, and facilitates preparation of homogeneous hydrogels. The calcium content of the dispersion can also be varied to adjust mechanical properties.

Therefore, the present formulation combines three features that have not previously been investigated together in our hydrogel systems: (i) sodium alginate as an ionotropically gelled polysaccharide matrix, (ii) hydrolyzed collagen as a low-molecular-weight bioactive protein component, and (iii) LC-PAA-Ca as a dispersed polymeric calcium-releasing

structuring agent. This combination provides a platform for investigating the influence of controlled calcium release and hydrolyzed collagen on hydrogel network formation and functional properties. Figure 2 illustrates the proposed formation of the hydrogel network through ionic and hydrogen-bonding interactions.

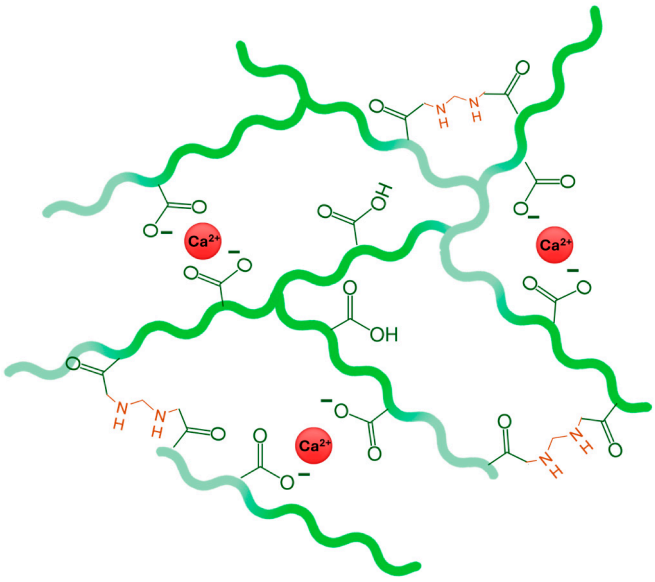


Figure 1. Schematic representation of the LC-PAA-Ca crosslinker.

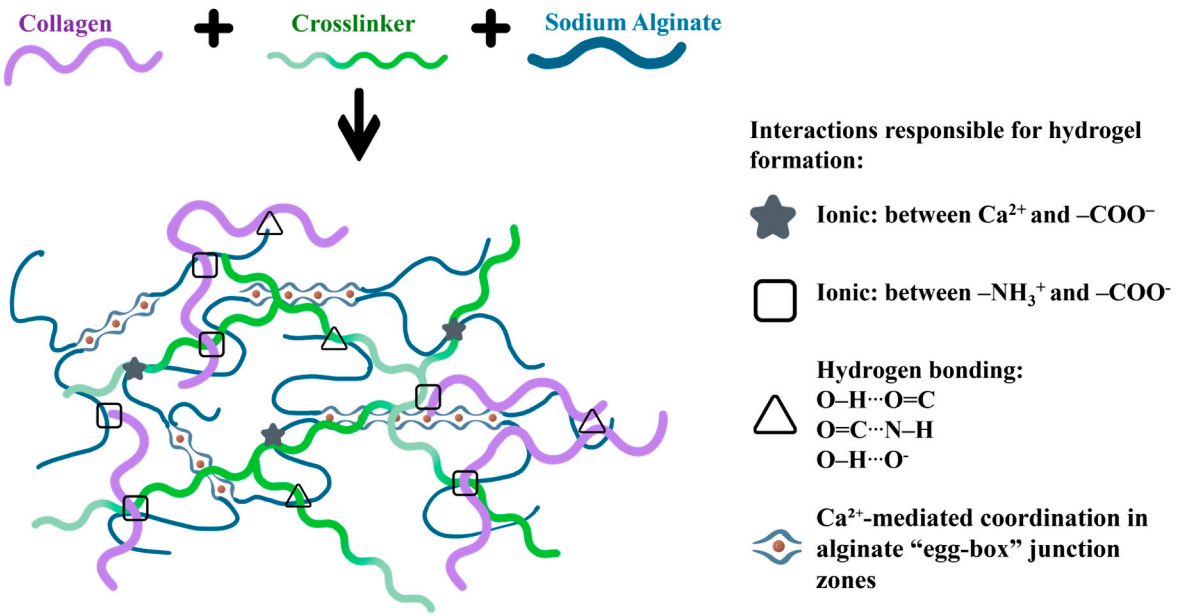


Figure 2. Proposed schematic representation of alginate–collagen hydrogel network formation and the associated noncovalent interactions.

Network formation involves Ca^{2+}-mediated ionic crosslinking, polyelectrolyte complex formation, hydrogen bonding, and physical chain entanglement. LC-PAA-Ca acts both as a Ca^{2+} source and as an additional polymeric framework. The principal gelation mechanism is coordination of Ca^{2+} ions between carboxylate groups of α-L-guluronic acid residues in sodium alginate. At the hydrogel-forming pH of 5.6–6.0, protonated amino groups of hydrolyzed collagen can interact electrostatically with free carboxylate groups of alginate and poly(acrylic acid). Numerous hydroxyls, amid, amino, and carboxyl groups may additionally

promote hydrogen bonding. Linear alginate chains and collagen molecules interpenetrate the microgel domains formed by LC-PAA. Glycerol and PEG-400 act as plasticizers, whereas HPMC regulates viscosity and stabilizes the LC-PAA/LC-PAA-Ca dispersion.

The formulation ranges and component ratios are reported in Table 2; sample 5 did not form a hydrogel network. The composition of the investigated hydrogels is summarized in Table 2, while their swelling characteristics and gel-fraction values are presented in Table 3a,b.

Table 3. (**a**) Swelling (T = 20 °C) and gel fraction characteristics of alginate–collagen hydrogels. (**b**) Swelling (T = 36 °C) of alginate–collagen hydrogels.

(**a**)

Characteristic	Swelling in Water, 20 °C (%, Relative to the Initial Hydrogel Mass)			Swelling in Exudate, 20 °C (%, Relative to the Initial Hydrogel Mass)			Gel Fraction, %
Time, h	3	24	144	3	24	144	-
Sample 1	291.6 ± 23.4	386.6 ± 63.6	428.1 ± 61.4	131.8 ± 16.9	128.4 ± 16.3	126.0 ± 16.0	78.2 ± 4.9
Sample 2	272.4 ± 35.3	428.0 ± 59.9	501.0 ± 11.2	66.3 ± 6.6	64.8 ± 6.5	59.6 ± 6.2	45.3 ± 3.7
Sample 3	280.7 ± 15.3	373.9 ± 41.7	403.3 ± 48.9	122.3 ± 43.1	117.7 ± 39.8	123.6 ± 41.8	42.8 ± 3.9
Sample 4	241.1 ± 39.6	293.8 ± 36.8	326.0 ± 54.0	132.8 ± 5.0	122.6 ± 6.4	126.4 ± 6.6	35.4 ± 2.4
Sample 6	344.0 ± 38.1	390.3 ± 35.6	416.2 ± 33.3	138.4 ± 8.5	134.1 ± 7.0	125.5 ± 1.3	42.4 ± 3.5
Sample 7	451.5 ± 27.2	502.7 ± 16.6	511.8 ± 28.1	171.4 ± 9.3	163.8 ± 4.7	157.4 ± 4.4	50.4 ± 2.1
Sample 8	343.9 ± 50.8	421.5 ± 37.3	476.4 ± 58.9	196.1 ± 18.1	177.6 ± 9.3	168.1 ± 15.6	44.5 ± 0.6
Sample 9	425.7 ± 48.1	538.0 ± 26.8	569.2 ± 33.6	190.0 ± 7.4	173.0 ± 20.5	169.4 ± 15.9	65.9 ± 4.3

(**b**)

Characteristic	Swelling in Water, 36 °C (%, Relative to the Initial Hydrogel Mass)			Swelling in Exudate, 36 °C (%, Relative to the Initial Hydrogel Mass)		
Time, h	3	24	148	3	24	148
Sample 1	240.9 ± 52.0	316.0 ± 56.4	328.5 ± 58.7	126.9 ± 12.3	115.1 ± 11.1	112.1 ± 10.9
Sample 2	353.3 ± 18.0	496.2 ± 2.6	504.0 ± 2.3	70.8 ± 3.4	57.8 ± 2.8	54.6 ± 2.6
Sample 3	452.3 ± 13.9	528.6 ± 28.5	485.8 ± 21.0	153.4 ± 3.2	144.5 ± 3.0	143.2 ± 3.0
Sample 4	314.1 ± 14.5	337.6 ± 18.4	249.4 ± 14.6	154.1 ± 3.1	138.2 ± 2.8	141.4 ± 2.8
Sample 6	295.4 ± 17.5	320.1 ± 7.7	210.1 ± 21.9	122.5 ± 3.9	115.0 ± 10.8	109.3 ± 20.3
Sample 7	385.0 ± 6.1	412.4 ± 14.1	250.3 ± 18.9	135.1 ± 5.6	124.7 ± 6.2	118.2 ± 25.8
Sample 8	318.3 ± 1.1	335.0 ± 23.8	205.7 ± 62.0	130.4 ± 2.3	128.0 ± 2.1	121.5 ± 3.7
Sample 9	390.2 ± 19.5	470.8 ± 5.5	289.5 ± 83.5	136.8 ± 14.1	112.3 ± 15.5	110.6 ± 18.5

3.1. Gel Fraction and Structural Characterization of Alginate–Collagen Hydrogels

The insoluble polymer-network content, expressed as the gel fraction (G_f, %), provides a quantitative measure of three-dimensional network formation and hydrogel stability in liquid media. Extraction for 24 h at 45 °C in a large excess of water revealed composition-dependent differences in polymer-network formation, as summarized in Table 3a. Two groups of samples were considered. In samples 1–4, the sodium alginate concentration was nearly constant, whereas the hydrolyzed collagen content increased from 0 to 14.62 wt.%. The gel fraction decreased monotonically from 78.19 ± 4.9% for sample 1 to 35.36 ± 2.4% for sample 4 (Table 3a). This trend indicates that the low-molecular-weight peptide fragments of hydrolyzed collagen contributed less effectively to Ca^{2+}-mediated ionic crosslinking than alginate. Collagen was retained mainly through electrostatic interactions between amino groups and free polymer carboxylates, together with comparatively weak hydrogen bonding. During exhaustive extraction, unbound water-soluble components were removed from the matrix. As the collagen content increased, the proportion of its unbound low-molecular-weight fragments increased, resulting in a decrease in G_f. The highest G_f value was obtained for collagen-free sample 1, in which Ca^{2+} ions could coordinate readily with available alginate carboxylate groups to form an ionotropic “egg-box” network.

To examine intermolecular interactions independently of total polymer content, samples 2, 6, 7, 8, and 9 were compared. These formulations contained approximately 6.95 wt.% total gel-forming polymers and similar amounts of auxiliary components but differed in the sodium alginate-to-collagen mass ratio. The dependence of G_f on this ratio is shown in Figure 3.

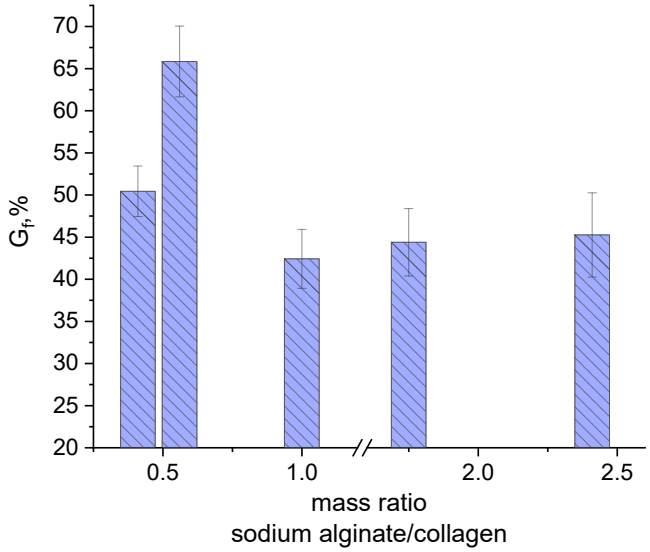


Figure 3. Gel fraction as a function of the sodium alginate-to-collagen mass ratio for samples 2 and 6–9 listed in Table 1.

A pronounced maximum was observed for sample 9 (G_f = 65.85%) at an alginate-to-collagen mass ratio of 0.56. While gravimetric gel-fraction data alone cannot provide direct molecular-level evidence, this nonmonotonic behavior can be tentatively interpreted through a balanced model that considers the interplay between a hypothetical redistribution of Ca^{2+}-mediated linkages and the formation of a dense cooperative hydrogen-bonding network. At higher alginate contents (samples 2, 6, and 8), a preferential binding of Ca^{2+} by the alginate macromolecular chains might theoretically alter the spatial arrangement of the adjacent LC-PAA-Ca domains, leading to an increased soluble fraction and yielding lower G_f values of 42.42–45.26%. As the alginate fraction decreases and the hydrolyzed collagen content increases (samples 7 and 9), it is reasonable to assume that the competition for Ca^{2+} coordination is modified. This reduction in ionic competition likely allows electrostatic an polyelectrolyte interactions may become increasingly important between the LC-PAA carboxylates and protonated amino groups of the collagen fragments become more prominent [37].

This proposed mechanism is structurally supported by complementary FTIR data (discussed in detail in Section 3.2), which revealed a significant bathochromic shift in the -OH/-NH stretching region (3600–3200 cm^{-1}). Semi-empirical evaluation of these spectral shifts yields an average hydrogen bond energy approximately equal to 18.5–22.4 kJ/mol and donor–acceptor distance R approximately equal to 2.76–2.81 Å.

At a mass ratio of 0.56 (sample 9), the synergy between these moderately strong hydrogen bonds and the residual ionic crosslinks appears to dynamically favor the most effective entrapment of the polymer components within the insoluble network. Further increasing the collagen content (sample 7; ratio 0.41) decreased G_f to 50.44%, presumably because excess low-molecular-weight peptide fragments exceeded the physical retention capacity of the interpenetrating matrix and were washed away into the sol fraction.

Consequently, while the integrated FTIR and gravimetric data provide a highly cohesive qualitative model for the stabilization of the developed hydrogels, definitive validation of the internal calcium ion redistribution remains a subject for future specialized spectroscopic and crosslinking density investigations.

3.2. Fourier Transform Infrared Spectroscopy—FTIR

FTIR spectroscopy was used to assess incorporation of sodium alginate and hydrolyzed collagen into the insoluble polymer network of samples 1–4. Figures 4 and 5 show the spectra over 4000–500 cm^{-1} and the fingerprint region of 1950–600 cm^{-1}, respectively.

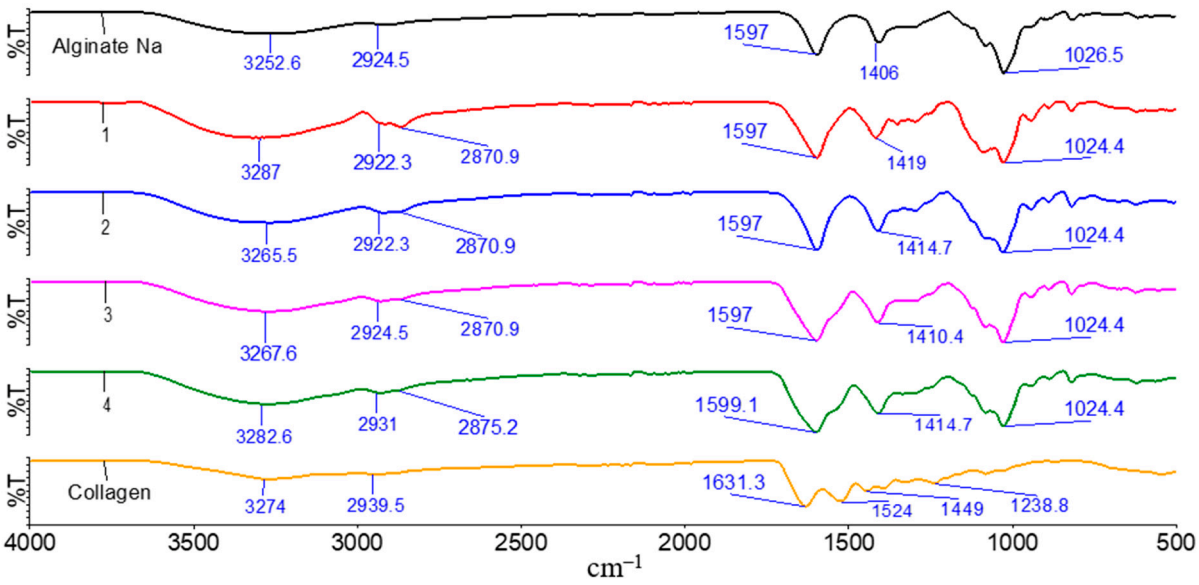


Figure 4. FTIR spectra of sodium alginate, collagen, and the gel-fraction polymers of alginate–collagen hydrogel samples 1–4 (Table 1) over 4000–500 cm^{-1}.

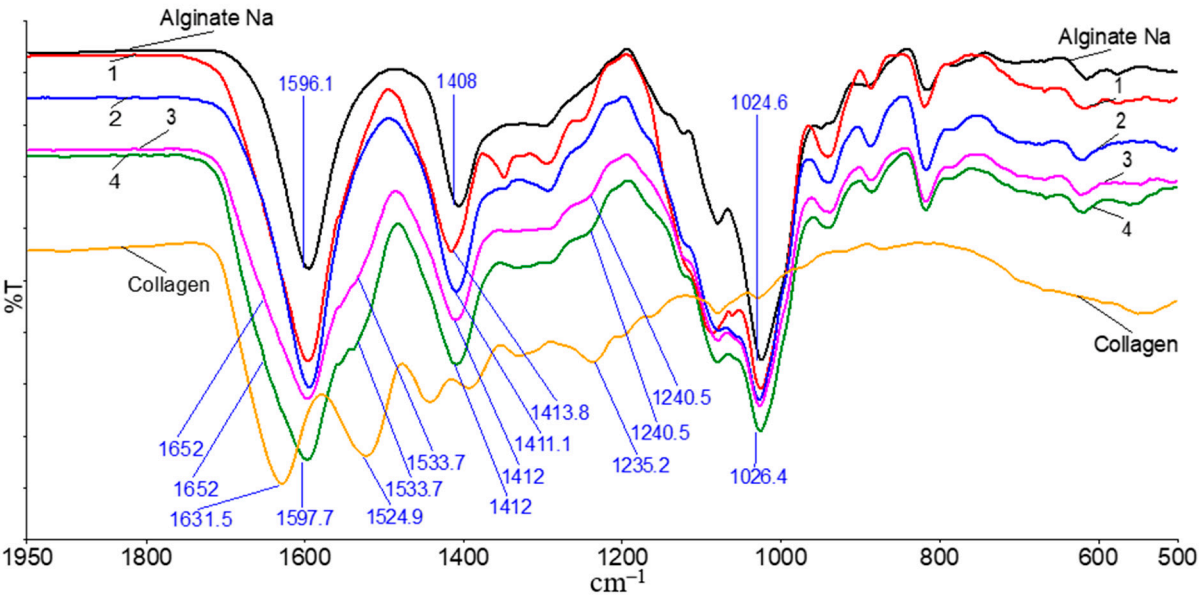


Figure 5. FTIR spectra of sodium alginate, collagen, and the gel-fraction polymers of alginate–collagen hydrogel samples 1–4 (Table 1) over 1950–500 cm^{-1}.

Pure hydrolyzed collagen exhibited characteristic absorption bands at 1629.68 cm^{-1} and 1522.14 cm^{-1}, which are conventionally assigned to Amide I (primarily C=O stretching)

and Amide II (coupled N-H in-plane bending and C-N stretching) vibrations of the peptide backbone, respectively, and at 1236.10 assigned to Amide III (coupled C-N stretching, N-H bending, and contributions from adjacent CH_2 wagging). Pure sodium alginate displayed its signature asymmetric and symmetric carboxylate -COO- stretching bands at 1595.67 cm^{-1} and 1406.38 cm^{-1}, alongside skeletal C-O-C and C-O stretching vibrations in the region of 1300–1000 cm^{-1} specifically at 1023.59 cm^{-1} corresponds to the C–O and C–O–C stretching vibrations. The Fourier-transform infrared (FTIR) spectra of the extracted polymeric hydrogel networks (samples 1–4) generally coincide with the spectrum of sodium alginate. A detailed interpretation of molecular interactions becomes intricate due to the extensive spectral overlapping of the carbonyl/carboxylate groups from both alginate and the LC-PAA matrix with the amide bands of the collagen fragments. Nevertheless, systematic spectral changes were observed.

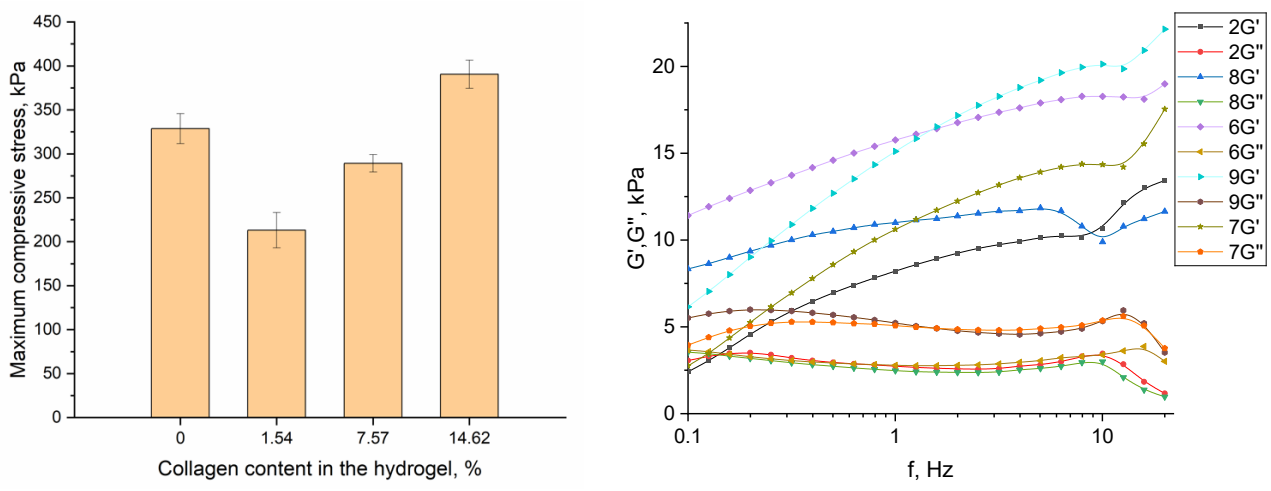
The wide, intense absorption band spanning 3600–3100 cm^{-1} with a maximum in the 3270 cm^{-1} is governed by the overlapping stretching vibrations of hydroxyl -OH groups from the polysaccharide/plasticizer matrix (at 3253 cm^{-1} in alginate) and amino -NH groups from the collagen peptide backbones (Amide A band at 3275 cm^{-1}). The Amide B band in the 3080–3090 cm^{-1} range corresponds to N–H stretching vibrations. The peak in the 2930–2865 cm^{-1} range is characteristic of C–H bonds, which are present in both proteins and polysaccharides.

The carboxylate bands of the polysaccharide component shifted slightly to 1597 cm^{-1} and 1410 cm^{-1}. Although these shifts to higher wavenumbers are relatively small (3–5 cm^{-1}), their reproducibility across the sample series reflects altered local electrostatic environments, consistent with weak polyelectrolyte or hydrogen bonding interactions between the alginate/LC-PAA carboxylates and the protonated amino or hydroxyl groups of the collagen chain. These high-frequency shifts suggest a reorganization of the native intra- and intermolecular hydrogen bonding network within the denatured collagen peptides, driven by the restriction of their segmental mobility within the crosslinked matrix due to conformational backbone compression.

In addition to these shifts, the band corresponding to the asymmetric vibrations of the carboxylate group at 1597 cm^{-1} in the obtained samples appears with shoulders on either side, as shown in Figure 5. This overlap, manifested as shoulders at 1653 and 1533 cm^{-1}, originates from the contribution of collagen Amide I and Amide II bands (Figure 5). Another indication of the presence of collagen in the obtained samples is an absorption shoulder at 1238 cm^{-1}, which corresponds to Amide III vibrations.

3.3. Mechanical and Rheological Properties

The mechanical response of samples 1–4 under uniaxial loading showed a nonlinear dependence of maximum stress at failure on hydrolyzed collagen content (Figure 6a). Addition of 1.54 wt.% collagen (sample 2) decreased the strength from 328 to 213 kPa, consistent with steric interference by collagen molecules that reduced the efficiency of Ca^{2+}-mediated alginate crosslinking. This trend is agreed with the decrease in G_f from 78.19 to 45.26%. Increasing the total polymer content to 19.70 wt.% by further increasing the collagen concentration in samples 3 and 4 raised the strength to 391 kPa. Although these samples exhibited comparatively low G_f values of 42.77 and 35.36%, respectively, the high collagen content may have promoted formation of a dense physical matrix stabilized by hydrogen bonding and electrostatic interactions. This matrix showed limited swelling and comparatively high resistance to mechanical loading.



(**a**) (**b**)

Figure 6. (**a**) Effect of collagen content on the maximum compressive stress of alginate–collagen hydrogels for samples 1–4 (data are presented as mean ± SD (n = 3)); (**b**) frequency dependence of G' and G'' for samples 2, 6, 7, 8, and 9 (Table 1).

Dynamic mechanical measurements for the isoconcentration series (samples 2, 6, 7, 8, and 9) are shown in Figure 6b. The storage modulus G' exceeded the loss modulus G'' over the entire frequency range of 0.1–20 Hz for all samples, demonstrating predominantly elastic behavior. Sample 9 exhibited the highest G' values, 15–22.5 kPa, consistent with its maximum G_f of 65.85%. Samples 2 and 8, which contained more sodium alginate, and sample 7, which contained more collagen, exhibited lower G' profiles. For samples 2 and 8, preferential allocation of Ca^{2+} bridges to alginate may weaken the LC-PAA network. For sample 7, unbound short collagen chains may exert a plasticizing effect and reduce interchain cohesion. Values of G'' remained below 6 kPa and tended to decrease or stabilize at high frequencies, indicating comparatively low mechanical-energy dissipation. Overall, the rheological response was consistent with the extraction results: higher effective network density was associated with higher G_f and greater elastic stiffness.

The balance between elastic and viscous behavior was evaluated using the loss factor, $\tan \delta = G''/G'$, as a function of the sodium alginate-to-collagen mass ratio (Figure 7).

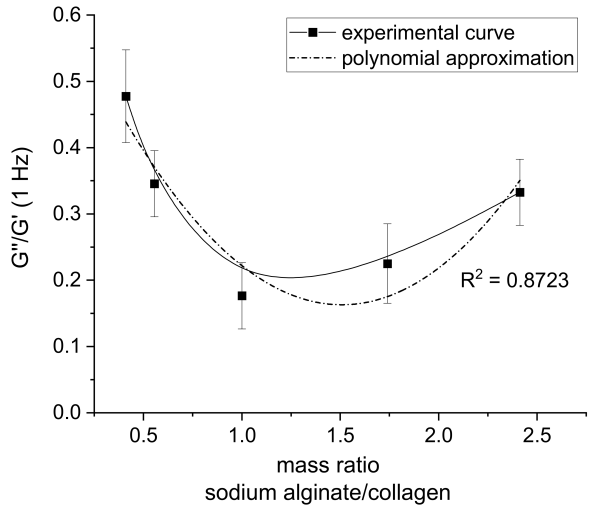


Figure 7. Loss factor as a function of the alginate-to-collagen mass ratio for samples 2, 8, 7, 6, and 9 (experimental data points are shown as mean ± SD (n = 3) with a polynomial approximation curve R^2 = 0.8723).

The data were described by a second-order polynomial relationship ($R^2 = 0.8723$). Across the isoconcentration series, tan δ ranged from 0.17 to 0.48. Because tan δ remained below 1, the elastic contribution predominated in all samples. The minimum value, tan $\delta = 0.17$, was observed at a 1:1 polymer ratio (sample 6), indicating the strongest predominance of elastic over viscous behavior. Departures from this ratio in either direction increased the loss factor.

3.4. Swelling Behavior of Alginate–Collagen Hydrogels

Swelling was investigated in distilled water and simulated wound exudate at 20 and 36 °C for up to 144–148 h using hydrated hydrogel matrices. This approach enabled evaluation of liquid uptake while accounting for simultaneous diffusion into the network and leaching of water-soluble components. As summarized in Table 3a,b, the degree of swelling, α (%), depended on total gel-forming polymer concentration, the sodium alginate-to-hydrolyzed collagen mass ratio, and network density as reflected by G_f.

For samples 1–4, the sodium alginate concentration remained within 3.48–3.74 wt.%, whereas the collagen content increased from 0 to 14.62 wt.% and the total polymer concentration increased from 5.46 to 19.70 wt.%. In water at 20 °C, addition of 1.54 wt.% collagen (sample 2) increased swelling to 501.0 ± 11.2% after 144 h, compared with 428.1 ± 61.4% for collagen-free sample 1. This increase may reflect disruption of close alginate-chain packing and the hydrophilicity of collagen amino groups. Further increases in collagen content reduced swelling to 326.0 ± 54.0% for sample 4, consistent with the lower gel fraction and with formation of a dense assembly of chains stabilized by numerous weak interactions that restricted network expansion and water transport.

The isoconcentration series (samples 2, 6, 7, 8, and 9) contained approximately 6.95 wt.% total gel-forming polymers but differed in biopolymer ratio. Sample 8 (ratio 1.75) exhibited moderate swelling, consistent with a predominantly Ca^{2+}-crosslinked alginate network. Sample 6 (ratio 1.0) showed balanced sorption behavior. Samples 7 and 9 (ratios 0.41 and 0.56, respectively) exhibited the highest water uptake at 20 °C, reaching 511.8 ± 28.1% and 569.2 ± 33.6%, respectively, which was associated with the larger fraction of hydrophilic collagen chains and greater conformational mobility of the network.

For all samples, swelling in simulated wound exudate was approximately 3- to 5-fold lower than that observed in distilled water, with equilibrium swelling values generally stabilizing within the range of 50–170%. That behavior is attributable to ionic screening of negatively charged carboxylate groups in alginate and LC-PAA, which decreases electrostatic repulsion and osmotic driving forces within the polyelectrolyte network. Increasing the temperature from 20 to 36 °C accelerated mass transfer, and most samples approached a sorption plateau within 3–24 h. During prolonged exposure to water at 36 °C, samples 6–9 showed a decrease in mass between 24 and 148 h, consistent with partial loss of network junctions and extraction of the sol fraction. In simulated wound exudate at 36 °C, all hydrogels retained their overall integrity up to 148 h.

It is critical to acknowledge the intrinsic limitations of the gravimetric swelling determination within these multi-component formulations. Because the initial hydrogel matrices are loaded with significant payloads of hydrophilic plasticizers (glycerol and PEG-400), the dynamic values reported in Table 3a,b represent a mechanistic gross effect (apparent sorption capacity). During the initial hours of exposure (3–24 h), the osmotic pressure driving water into the highly hydrophilic matrix heavily dominates, yielding a sharp upward kinetic profile.

However, over extended incubation times, especially at the physiological temperature of 36 °C, the exhaustive extraction of uncrosslinked low-molecular-weight components and plasticizers into the large excess of water begins to outpace or flatten the net fluid

absorption. This mass-transfer imbalance structurally rationalizes the observed drop in apparent swelling for several formulations at 144 h. While this gravimetric approach cannot independently distinguish the isolated kinetics of component loss from pure water uptake, this simulated model serves as a highly realistic indicator of the material's behavior under real-world clinical application conditions, capturing the total, non-ideal mass redistribution that occurs when a fully assembled wound dressing encounters external biological fluids.

3.5. Release of Hydrolyzed Collagen from Composite Hydrogels into Simulated Wound Exudate

The release of hydrolyzed collagen into simulated wound exudate was examined to characterize mass transport from the composite hydrogels and to assess their potential to provide either rapid or prolonged collagen delivery (Figure 8). Released low-molecular-weight collagen peptides have been reported to support processes relevant to wound repair, including fibroblast and keratinocyte migration, re-epithelialization, and modulation of excessive matrix metalloproteinase activity [38,39].

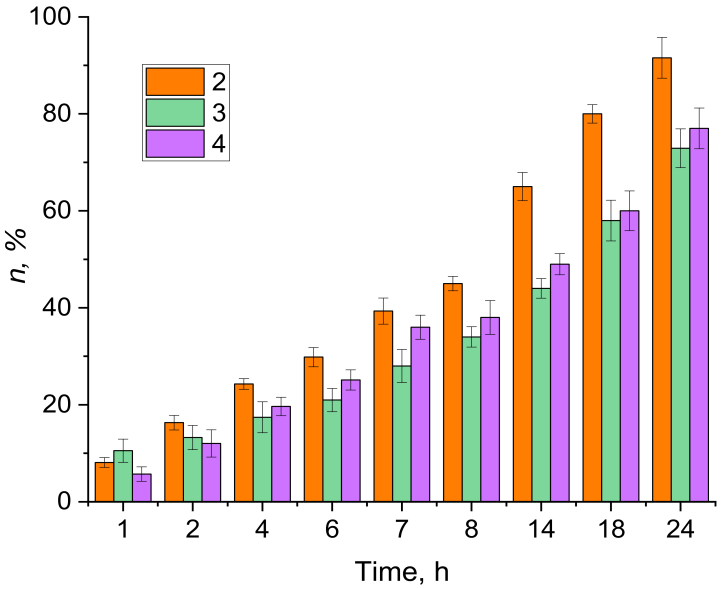


Figure 8. Collagen release from alginate–collagen hydrogel samples 2–4 (Table 1) as a function of time (each bar represents the mean value ± SD ($n = 3$).

During the first 7 h, samples 2–4 released approximately 30–40% of their collagen, which was attributed primarily to diffusion of weakly retained peptides from near-surface regions and provided an initial release phase. After 24 h, collagen release reached approximately 92% for sample 2 and approximately 73% for samples 3 and 4. The faster and more complete release from sample 2 was consistent with its hydrophilic, relatively mobile, alginate-rich network, which promoted pore expansion during exudate uptake and thereby facilitated collagen diffusion. In samples 3 and 4, the higher collagen concentration likely increased physical chain entanglement and slowed diffusion despite their lower gel fractions, producing a more prolonged release profile. Thus, sample 2 may be more suitable when rapid collagen delivery is required, whereas samples 3 and 4 may provide more sustained release. These results demonstrate that matrix composition can be used to modulate collagen-release kinetics, although the associated biological effects require separate experimental verification.

To further elucidate the mechanism of collagen release, the experimental data were analyzed using zero-order, first-order, Higuchi, Hixson–Crowell, and Korsmeyer–Peppas

kinetic models. The corresponding kinetic plots are provided in Figures S1–S5 while the calculated kinetic parameters are summarized in Table 4.

Table 4. Kinetic parameters of collagen release from alginate–collagen hydrogels.

Sample (Table 2)	Zero Order		First Order		Higuchi Kinetics		Hixson–Crowell		Korsmeyer–Peppas		
	k_0 (h^{-1})	R^2	k_1 (h^{-1})	R^2	k_H ($h^{-1/2}$)	R^2	k_{HC} (h^{-1})	R^2	K (h^{-n})	n	R^2
Sample 2	3.4712	0.9855	0.0099	0.9805	14.627	0.9342	0.0657	0.9893	0.0777	0.6104	0.986
Sample 3	2.8686	0.9903	0.0085	0.9834	13.524	0.9254	0.058	0.9909	0.0600	0.6782	0.9948
Sample 4	2.6701	0.9941	0.0172	0.9591	17.842	0.9448	0.0983	0.9798	0.1143	0.5402	0.9992

All formulations showed relatively high coefficients of determination ($R^2 > 0.92$) for the tested models, suggesting that several kinetic models can adequately describe the experimental release profiles. The lowest correlation coefficients were obtained for the Higuchi model ($R^2 = 0.9254$–0.9448), suggesting that simple Fickian diffusion through a non-swelling matrix cannot fully explain the observed release behavior.

The Korsmeyer–Peppas model provided the best overall description of the release profiles for samples 3 and 4, yielding R^2 values of 0.9948 and 0.9992, respectively. Comparable agreement between the Korsmeyer–Peppas and Hixson–Crowell models was observed for sample 2. These results indicate that, besides diffusion, changes in the hydrogel structure may contribute to collagen transport.

The release exponent n obtained from the Korsmeyer–Peppas model ranged from 0.5402 to 0.6782 for all investigated formulations. Since these values fall within the range $0.45 < n < 0.89$, collagen release can be classified as anomalous (non-Fickian) transport. Therefore, collagen release is controlled by a combination of diffusion through the hydrated alginate–collagen network and relaxation/swelling of the hydrogel matrix. This interpretation is consistent with the swelling behavior observed in simulated wound exudate.

Although increasing collagen loading affected the release rate constants and the total amount released within 24 h, the values of n remained within the same transport regime. This observation suggests that variations in collagen content influence the rate of release rather than the fundamental release mechanism.

3.6. Cytotoxicity Assessment of Alginate–Collagen Hydrogel

For hydrogel materials intended for wound treatment, evaluation of cytotoxicity is essential due to their direct contact with injured tissues.

Based on literature data, the individual components (sodium alginate, collagen, HPMC, glycerol, and PEG-400) comprising the hydrogel are considered biocompatible and non-cytotoxic [40–44]. The LC-PAA and its calcium salt used in this study are structural and functional analogues of pharmaceutical-grade poly(acrylic acid) (known as Carbomer or Carbopol) and its salts, which exhibit no cellular toxicity [36,45,46]. Accordingly, a similar absence of toxicity can be reasonably assumed for the LC-PAA polymer employed in hydrogel synthesis. In its crosslinked (lightly crosslinked) state, this polymer possesses a high molecular weight and a three-dimensional network architecture, rendering it biologically inert and incapable of penetrating cell membranes or entering the systemic circulation.

Nevertheless, a comprehensive assessment of the developed alginate–collagen material was performed using an alternative in vitro cell model, namely bull spermatozoa [47]. Although this model cannot fully replicate the complex microenvironment of healing skin tissue, mammalian spermatozoa represent a highly sensitive and reliable platform for the initial screening of general cytotoxicity. Due to their intense metabolic activity, precise motility, and vulnerable plasma membranes, these cells rapidly respond to the presence of toxic leachable substances or adverse physicochemical shifts. Sample 2 was selected for

the studies as it is representative of the entire hydrogel series, given that the qualitative composition is identical and variations pertain only to the ratio of structural polymers (alginate and collagen). Since Sample 2 did not cause statistically significant reductions in cell survival relative to the control ($p > 0.05$), this formulation can be regarded as non-cytotoxic within the limitations of the applied model. Although all investigated hydrogels share the same qualitative composition, only Sample 2 was evaluated experimentally. Therefore, the present results support the cytocompatibility of the investigated formulation but should not be interpreted as direct evidence for all hydrogel compositions.

Based on these results (Table 5), the investigated alginate–collagen hydrogel sample in the concentration range of 10–50 mg/mL is biocompatible and exhibits no direct cytotoxic action, as evidenced by the absence of reduced cell survival relative to the control. However, the material induces a pronounced metabolic rearrangement in cells. A dose-dependent inhibition of cytochrome oxidase (COX) activity, reaching 59.1% at 50 mg/mL, is observed, accompanied by a compensatory 1.7-fold increase in succinate dehydrogenase (SDH) activity. This metabolic shift suggests an alteration in energy pathways, specifically transitioning towards the succinate oxidase respiratory route. In mammalian cells, this alternative pathway allows for faster ATP resynthesis compared to the terminal chain, which could theoretically support the accelerated energetic demands of damaged tissues during regenerative processes. While this interaction highlights a potentially active role of the hydrogel matrix in modulating cell metabolism, a cautious interpretation is strictly necessary.

Table 5. Survival and oxidative enzyme activity of bull spermatozoa upon contact with the hydrogel sample, $n = 4$.

Conditions	Dose, mg/mL	Parameters					
		Survival *, h		COX, U		SDH, U	
		M ± m	CV	M ± m	CV	M ± m	CV
Control	-	101.0 ± 4.20	10.1	49.7 ± 6.20	22.2	13.7 ± 3.68	58.4
Sample 2 from Table 1	10	96.0 ± 5.00	9.1	39.7 ± 5.01	24.8	19.7 ± 5.44	53.9
	20	100.0 ± 5.20	11.1	39.0 ± 7.16	36.4	19.6 ± 5.04	58.6
	50	97.0 ± 4.20	10.2	20.3 ± 3.72	20.2	23.3 ± 6.20	53.7
η		0.40		0.75		0.41	

* Cytotoxicity analysis based on the retention of sperm motility was performed at varying intervals: every 24 h when up to 50% of cells exhibited progressive motility, every 12 h when this figure was up to 10%, and hourly when the value fell below 10%.

It must be acknowledged that these biological findings are subject to certain limitations. Only Sample 2 was evaluated experimentally; therefore, the obtained results confirm the absence of measurable cytotoxic effects for this formulation only and should not be directly extrapolated to the entire hydrogel series. Although all investigated hydrogels share the same qualitative composition, differences in the alginate-to-collagen ratio may affect network organization and material–cell interactions. Consequently, cytocompatibility testing of the remaining formulations is required. Furthermore, the spermatozoa model cannot reproduce the complexity of wound-healing processes, and additional studies using relevant skin-cell models and in vivo systems are necessary to validate the biomedical potential of the developed hydrogels.

4. Conclusions

A series of hydrogels were synthesized as interpenetrating polymer networks (IPNs) formed by combining sodium alginate, hydrolyzed collagen, HPMC, and the calcium salt of lightly crosslinked poly(acrylic acid) (LC-PAA-Ca). Investigation of an isoconcentration

series containing 6.95–6.98 wt.% of gel-forming polymers demonstrated that the alginate-to-collagen mass ratio significantly influences network formation, rheological behavior, swelling characteristics, and collagen release. These results confirm that the structural and functional properties of the developed hydrogels can be adjusted through changes in biopolymer composition.

Gel-fraction analysis revealed a nonmonotonic dependence of network formation on hydrogel composition. The maximum gel fraction was observed for sample 9 ($65.85 \pm 4.30\%$) at an alginate-to-collagen mass ratio of 0.56, indicating the most efficient retention of polymer components within the insoluble network among the investigated formulations. Rheological measurements showed that all hydrogels exhibited predominantly elastic behavior ($G' > G''$), while sample 9 displayed the highest storage modulus (15–22.5 kPa), suggesting the greatest network stiffness. In contrast, sample 6 showed the lowest loss factor, indicating the strongest predominance of elastic over viscous behavior.

The swelling behavior strongly depended on hydrogel composition and the swelling medium. In simulated wound exudate, all formulations exhibited substantially lower swelling than in distilled water due to ionic screening effects, while maintaining structural integrity for up to 148 h at 36 °C. Collagen release studies showed that the release rate could be adjusted through formulation design, whereas kinetic analysis indicated anomalous (non-Fickian) transport governed by the combined contributions of diffusion and matrix relaxation processes.

Among the investigated formulations, sample 9 appears to be the most balanced composition based on the combined physicochemical dataset obtained in this study. This formulation simultaneously exhibited the highest gel fraction, the highest storage modulus, and one of the highest swelling capacities in water ($569.2 \pm 33.6\%$), indicating a favorable combination of network integrity, mechanical stability, and fluid uptake capability.

Nevertheless, the present conclusions are limited to physicochemical characterization, collagen-release studies, and preliminary in vitro cytocompatibility assessment. Although the obtained results suggest that the developed hydrogels may be considered promising candidates for further investigation as wound-dressing materials, their practical biomedical applicability cannot be confirmed at this stage. Additional studies, including expanded biocompatibility testing using relevant skin-cell models, in vivo wound-healing evaluation, long-term storage stability assessment, and sterility studies, are required to establish their suitability for clinical or commercial applications.

Supplementary Materials: The following supporting information can be downloaded at: https://www.mdpi.com/article/10.3390/jcs10110607/s1, Figures S1–S5: Kinetic modeling of collagen release from alginate–collagen hydrogels (Samples 2–4) using zero-order (S1), first-order (S2), Higuchi (S3), Hixson–Crowell (S4), and Korsmeyer–Peppas models (S5).

Author Contributions: Conceptualization, N.N., S.V. and V.S.; methodology, N.B. and O.B.; validation, S.K. (Solomiia Kapatsila), A.S., R.T. and D.O.; formal analysis, N.N.; investigation, Y.C. and S.K. (Semen Khomyak); resources, A.S.; data curation, N.N. and O.M.; writing—original draft preparation, N.N.; writing—review and editing, S.V. and O.M.; visualization, S.K. (Solomiia Kapatsila), N.N. and O.B.; supervision, V.S.; project administration, S.V.; funding acquisition, V.S. All authors have read and agreed to the published version of the manuscript.

Funding: This research was funded by the NATIONAL RESEARCH FOUNDATION OF UKRAINE, state registration number 0124U003832.

Data Availability Statement: The raw data supporting the conclusions of this article will be made available by the authors on request. Further inquiries can be directed to the corresponding author.

Acknowledgments: The authors would like to express their gratitude to the ARMED FORCES OF UKRAINE for providing security to us and our families and the possibility to perform this work.

Conflicts of Interest: The authors declare no conflicts of interest.

References

1. Hosseini, S.A.; Noruzi, S.; Kesharwani, P.; Sahebkar, A. Hydrogel-Based Dressing for Wound Healing: A Systematic Review of Clinical Trials. *Int. J. Biol. Macromol.* **2025**, *308*, 142322. [CrossRef] [PubMed]
2. Mo, Y.; Zhou, T.; Li, W.; Niu, Y.; Sheu, C. Advances in Nanohybrid Hydrogels for Wound Healing: From Functional Mechanisms to Translational Prospects. *Gels* **2025**, *11*, 483. [CrossRef] [PubMed]
3. Grand View Research. Hydrogel Dressing Market Report. Available online: https://www.grandviewresearch.com/industry-analysis/hydrogel-dressing-market-report (accessed on 1 September 2026).
4. Sen, C.K. Human Wound and Its Burden: Updated 2020 Compendium of Estimates. *Adv. Wound Care* **2021**, *10*, 281–292. [CrossRef] [PubMed]
5. Alberts, A.; Moldoveanu, E.-T.; Niculescu, A.-G.; Grumezescu, A.M. Hydrogels for Wound Dressings: Applications in Burn Treatment and Chronic Wound Care. *J. Compos. Sci.* **2025**, *9*, 133. [CrossRef]
6. Ujjwal, R.R.; Yadav, A.; Tripathi, S.; Krishna, S.T.V.S. Polymer-Based Nanotherapeutics for Burn Wounds. *Curr. Pharm. Biotechnol.* **2022**, *23*, 1460–1482. [CrossRef] [PubMed]
7. Hurlow, J.; Bowler, P.G. Acute and Chronic Wound Infections: Microbiological, Immunological, Clinical and Therapeutic Distinctions. *J. Wound Care* **2022**, *31*, 436–445. [CrossRef] [PubMed]
8. Grytsenko, O.; Pukach, P.; Vovk, M.; Baran, N. Structural Features and Mechanical Properties of Hydrogels Based on PVP Copolymers, Obtained in the Presence of a Solvent. *Gels* **2025**, *11*, 1008. [CrossRef] [PubMed]
9. Hu, T.; Lo, A.C.Y. Collagen-Alginate Composite Hydrogel: Application in Tissue Engineering and Biomedical Sciences. *Polymers* **2021**, *13*, 1852. [CrossRef] [PubMed]
10. Mortier, C.; Costa, D.C.S.; Oliveira, M.B.; Haugen, H.J.; Lyngstadaas, S.P.; Blaker, J.J.; Mano, J.F. Advanced Hydrogels Based on Natural Macromolecules: Chemical Routes to Achieve Mechanical Versatility. *Mater. Today Chem.* **2022**, *26*, 101222. [CrossRef]
11. Vasile, C.; Pamfil, D.; Stoleru, E.; Baican, M. New Developments in Medical Applications of Hybrid Hydrogels Containing Natural Polymers. *Molecules* **2020**, *25*, 1539. [CrossRef] [PubMed]
12. Zhang, Y.; Huang, Y. Rational Design of Smart Hydrogels for Biomedical Applications. *Front. Chem.* **2021**, *8*, 615665. [CrossRef] [PubMed]
13. Suberlyak, S.; Petrina, R.; Grytsenko, O.; Baran, N.; Komar, A.; Berezhnyy, B. Investigation of the Sorption Capacity of Polyvinylpyrrolidone Copolymers as the Basis of Hydrogel Cosmetic Masks with Plant Biomass Extracts. *Chem. Chem. Technol.* **2022**, *16*, 555–563. [CrossRef]
14. Maikovych, O.V.; Nosova, N.H.; Yakoviv, M.V.; Dron, I.A.; Stasiuk, A.V.; Samaryk, V.Y.; Varvarenko, S.M.; Voronov, S.A. Composite Materials Based on Polyacrylamide and Gelatin Reinforced with Polypropylene Microfiber. *Vopr. Khim. Khim. Tekhnol.* **2021**, *134*, 45–54. [CrossRef]
15. Park, J.; De, R. Next-Generation Wound Healing Materials: Role of Biopolymers and Their Composites. *Polymers* **2025**, *17*, 2244. [CrossRef] [PubMed]
16. Rajinikanth, B.S.; Rajkumar, D.S.R.; Keerthika, K.; Vijayaragavan, V. Chitosan-Based Biomaterial in Wound Healing: A Review. *Cureus* **2024**, *16*, e55193. [CrossRef] [PubMed]
17. Shymborska, Y.; Tymetska, S.; Budkowski, A.; Zemła, J.; Raczkowska, J.; Awsiuk, K.; Bernasik, A.; Lekka, M.; Volinsky, A.A.; Pabijan, J.; et al. 'Smart' Polymer Sandwiches from Hydrogel Nanocoatings Attached to Stimuli-Responsive Grafted Brush Coatings: Changing the Cell Behavior. *J. Biomed. Mater. Res. Part B Appl. Biomater.* **2025**, *113*, e35631. [CrossRef] [PubMed]
18. Islam, M.M.; Shahruzzaman, M.; Biswas, S.; Sakib, M.N.; Rashid, T.U. Chitosan Based Bioactive Materials in Tissue Engineering Applications—A Review. *Bioact. Mater.* **2020**, *5*, 164–183. [CrossRef] [PubMed]
19. Maikovych, O.; Pasetto, P.; Nosova, N.; Kudina, O.; Ostapiv, D.; Samaryk, V.; Varvarenko, S. Functional Properties of Gelatin–Alginate Hydrogels for Use in Chronic Wound Healing Applications. *Gels* **2025**, *11*, 174. [CrossRef] [PubMed]
20. Vlizlo, V.; Ostapiv, D.; Kuzmina, N.; Mysak, A.; Nosova, N.; Varvarenko, S.; Samaryk, V.; Stybel, V.; Ostapiv, R. Sorptive Properties of Hydrogel Dressings and Their Antimicrobial Action After Saturation with Tetracyclines. *Regul. Mech. Biosyst.* **2025**, *16*, e25088. [CrossRef]
21. Servín de la Mora-López, D.; Olivera-Castillo, L.; López-Cervantes, J.; Sánchez-Machado, D.I.; Ayala-Zavala, J.F.; Soto-Valdez, H.; Madera-Santana, T.J. Bioengineered Chitosan–Collagen–Honey Sponges: Physicochemical, Antibacterial, and In Vitro Healing Properties for Enhanced Wound Healing and Infection Control. *Polymers* **2025**, *17*, 2379. [CrossRef] [PubMed]
22. Bielska, B.; Miłowska, K. Therapeutic Potential of Chitosan-Based and Related Nanocomposite Systems in Wound Management: A Review. *Int. J. Mol. Sci.* **2025**, *26*, 11748. [CrossRef] [PubMed]
23. Pintilei, P.S.; Binaymotlagh, R.; Chronopoulou, L.; Palocci, C. The Role of Natural Hydrogels in Enhancing Wound Healing: From Biomaterials to Bioactive Therapies. *Pharmaceutics* **2025**, *17*, 1243. [CrossRef] [PubMed]

24. Thang, N.H.; Chien, T.B.; Cuong, D.X. Polymer-Based Hydrogels Applied in Drug Delivery: An Overview. *Gels* **2023**, *9*, 523. [CrossRef] [PubMed]
25. Muñoz-Castiblanco, T.; Moreno-Marín, J.P.; Osorio, M. Natural Macromolecule-Based Bioinks for 3D Bioprinting: A Systematic Review of Composition, Physicochemical Characterization, and Biomedical Applications. *Bioprinting* **2025**, *48*, e00407. [CrossRef]
26. Bukartyk, M.M.; Nosova, N.G.; Maikovych, O.V.; Bukartyk, N.M.; Stasiuk, A.V.; Dron, I.A.; Varvarenko, S.M. Preparation and Research of Properties of Combined Alginate/Gelatin Hydrogels. *J. Chem. Technol.* **2022**, *30*, 11–20. [CrossRef]
27. Maikovych, O.; Nosova, N.; Bukartyk, N.; Fihurka, N.; Ostapiv, D.; Samaryk, V.; Pasetto, P. Gelatin-Based Hydrogel with Antiseptic Properties: Synthesis and Properties. *Appl. Nanosci.* **2023**, *13*, 7611–7623. [CrossRef]
28. Zheng, Z.; Qi, J.; Hu, L.; Ouyang, D.; Wang, H.; Sun, Q.; Lin, L.; You, L.; Tang, B. Cannabidiol-Containing Alginate-Based Hydrogel as Novel Multifunctional Wound Dressing for Promoting Wound Healing. *Biomater. Adv.* **2022**, *134*, 112560. [CrossRef] [PubMed]
29. Anjum, S.; Gurave, P.; Gupta, B. Calcium Ion Induced Self-Healing Pattern of Chemically Crosslinked Poly(Acrylic Acid) Hydrogels. *Polym. Int.* **2018**, *67*, 1148–1157. [CrossRef]
30. Kapatsila, S.; Taras, R.; Varchuk, D.; Nosova, N.; Varvarenko, S.; Samaryk, V. Influence of Calcium Crosslinker Form on Alginate Hydrogel Properties. *Gels* **2025**, *11*, 885. [CrossRef] [PubMed]
31. Malektaj, H.; Drozdov, A.D.; de Claville Christiansen, J. Mechanical Properties of Alginate Hydrogels Cross-Linked with Multivalent Cations. *Polymers* **2023**, *15*, 3012. [CrossRef] [PubMed]
32. Mazurek, Ł.; Kuś, M.; Jurak, J.; Rybka, M.; Kuczeriszka, M.; Stradczuk-Mazurek, M.; Konop, M. Biomedical Potential of Alginate Wound Dressings—From Preclinical Studies to Clinical Applications: A Review. *Int. J. Biol. Macromol.* **2025**, *309*, 142908. [CrossRef] [PubMed]
33. Alsaei, A.; Zarwi, A.; Binrajab, A.; Rahimi, F.; AlAnsari, R.; Kumar, M.P.; Butler, A.E.; Atkin, S.L.; Deen, G.R. Alginate-Based Biomaterials: From Fundamental "Egg-Box" Chemistry to Diverse Biomedical and Metabolic Management of Obesity and Diabetes. *Gels* **2026**, *12*, 250. [CrossRef] [PubMed]
34. Dierckx, S.; Patrizi, M.; Merino, M.; González, S.; Mullor, J.L.; Nergiz-Unal, R. Collagen Peptides Affect Collagen Synthesis and the Expression of Collagen, Elastin, and Versican Genes in Cultured Human Dermal Fibroblasts. *Front. Med.* **2024**, *11*, 1397517. [CrossRef] [PubMed]
35. Liang, X.; Chen, S.; Liang, Y.; Wang, M.; Wang, Q.; Chen, D.; Ma, X.; Ding, H.; Zhong, H.J. Alginate-Based Hydrogels: Recent Progress in Preparation, Property Tuning, and Multifunctional Applications. *Gels* **2026**, *12*, 182. [CrossRef] [PubMed]
36. Savić Gajić, I.M.; Savić, I.M.; Svirčev, Z. Preparation and Characterization of Alginate Hydrogels with High Water-Retaining Capacity. *Polymers* **2023**, *15*, 2592. [CrossRef] [PubMed]
37. Afrin, S.; Shahruzzaman, M.; Haque, P.; Islam, M.S.; Hossain, S.; Rashid, T.U.; Ahmed, T.; Takafuji, M.; Rahman, M.M. Advanced CNC/PEG/PDMAA Semi-IPN Hydrogel for Drug Delivery Management in Wound Healing. *Gels* **2022**, *8*, 340. [CrossRef] [PubMed]
38. Fleck, C.A.; Simman, R. Modern Collagen Wound Dressings: Function and Purpose. *J. Am. Coll. Certif. Wound Spec.* **2010**, *2*, 50–54. [CrossRef] [PubMed]
39. Choi, E.; Kim, M.; Lee, D.H.; Shim, S.; Kim, D.U.; Hong, J.M.; Chung, H.C. Functional Benefits of Low-Molecular-Weight Collagen Peptide in Achilles Tendon and Medial Collateral Ligament Injuries and Anterior Cruciate Ligament Transection-Induced Osteoarthritis. *J. Microbiol. Biotechnol.* **2025**, *35*, e2506035. [CrossRef] [PubMed]
40. Majidi, S.S.; Su, Y.; Jørgensen, M.L.; Muller, C.; Forooghi, P.; Nie, G.; Chen, M. Rayleigh Instability-Driven Coaxial Spinning of Knotted Cell-Laden Alginate Fibers as Artificial Lymph Vessels. *ACS Appl. Mater. Interfaces* **2021**, *13*, 22142–22149. [CrossRef] [PubMed]
41. Naik, K.; Vanina, A.S.; Srivastava, S.K.; Sychev, A.V.; Postnikov, E.B.; Parmar, A.S. Structural and Rheological Properties of a Fish Collagen-Based Hydrogel Considered as a Brain Tissue Phantom. *Langmuir* **2025**, *41*, 6124–6131. [CrossRef] [PubMed]
42. BenchChem Technical Support Team. *In Vitro Cytotoxicity of Hydroxyethyl Cellulose Compared to Other Common Cellulose Ethers: A Comparative Guide*; BenchChem: Ontario, CA, USA, 2025.
43. Alnuqaydan, A. *Determination of Cancer Induction and Cell-Killing Potential of Beauty Products and Personal Care Products Using Human Skin Cells*; Flinders University: Adelaide, Australia, 2011.
44. da S Reis, F.; de Sousa, W.V.; Luna, A.F.; de Melo, W.G.G.; Neto, M.A.; Rai, M.; Fialho, A.C.; Caland, J.; Ju, E.F.; Lima, F.; et al. Development of Scaffold Based on Buriti Oil and PEG-400 at Low Temperature. *ACS Omega* **2025**, *11*, 13023–13035. [CrossRef] [PubMed]
45. Hayati, F.; Ghamsari, S.M.; Dehghan, M.M.; Oryan, A. Effects of Carbomer 940 Hydrogel on Burn Wounds: An In Vitro and In Vivo Study. *J. Dermatol. Treat.* **2018**, *29*, 593–599. [CrossRef] [PubMed]

46. Ran, F.; Mu, K.; Liu, G.; Liu, Y.; Pang, Y.; Feng, G.; Zhou, L.; Peng, L. Preparation, Characterization, and Wound Healing Promotion of Hydrogels Containing Glucosyloxybenzyl 2-Isobutylmalates Extract from Bletilla striata (Thunb.) Reichb.f. *Int. J. Mol. Sci.* **2024**, *25*, 10563. [CrossRef]
47. Andersson, M.; Mikkola, R.; Kotiaho, M.; Hoornstra, D.; Salkinoja-Salonen, M. Boar Spermatozoa as a Tool in Toxicological Research, a Novel Application for Extended Boar Semen Commercially Produced by AI Stations. *Reprod. Domest. Anim.* **2006**, *41*, 303.

Disclaimer/Publisher's Note: The statements, opinions and data contained in all publications are solely those of the individual author(s) and contributor(s) and not of MDPI and/or the editor(s). MDPI and/or the editor(s) disclaim responsibility for any injury to people or property resulting from any ideas, methods, instructions or products referred to in the content.